

How do longitudinal waves propagate transversely?

P Huthwaite

24th June 2024

—

Acknowledgement: I prepared this paper in early 2021, and sent it to a journal for review. The reviewers correctly identified that this was, in fact, not an undiscovered phenomenon but that it was already known by areas of the community. In particular, a reference was given to [Catheline & Benech, "Longitudinal shear wave and transverse dilatational wave in solids", JASA 137, EL200-EL205 (2015)], and there were references within that dating back to the 1990s. The other reviewer stated that this had been known since 1956, and did not warrant a new publication. Any PhD students reading this can maybe learn about the value of good literature reviews! (Although finding appropriate keywords to search for in this case is likely to be a challenge.)

I am posting this paper here, with this acknowledgement that I am not claiming novelty, because I think it is an interesting and surprising result, which does not seem to be widely known (certainly it was new to anyone I spoke to about the problem). This phenomenon does appear and causes some confusion when using finite element methods.

—

Abstract

Modern, high-fidelity numerical simulations have shown an apparently anomalous result: a longitudinal elastodynamic wave travelling perpendicular to the forcing direction. Numerical simulations, in combination with an analytical model, are used to confirm that this is not simply a simulation artefact, but a true physical phenomenon, as well as illustrating that the behaviour also occurs for shear and guided waves. When assessing how this unexpected wave interacts with objects, however, it is found that it does not scatter, despite being clearly measurable. This paper has uncovered and explained this behaviour, which is critical for the reliable use of numerical wave simulations in elastic media, as well as potentially for high sensitivity experiments and other polarised wave modalities.

1 Introduction

A longitudinal wave excited in an elastic medium is defined as travelling in the same direction as the displacement within the wave. However, recent high-accuracy simulations have highlighted an apparent contradiction of this definition, showing that there is a small but measurable wave travelling at the longitudinal wave speed completely perpendicularly to the displacement direction, where only a shear wave (at different speed) would be expected to be present. Similarly, it is possible to identify a wave propagating at shear wave speed in the longitudinal direction.

Guided wave simulations demonstrate the same behaviour. An in-plane force excitation on the surface of the plate below the first cutoff frequency would be expected to excite the S_0 mode propagating along the direction of excitation (and a small amount of A_0), and SH_0 perpendicular to this, however, in both directions there appears to be a mixture of both S_0 and SH_0 .

The identification of these waves has only been possible through the use of high-fidelity numerical methods for ultrasonic simulation in solids, in particularly the finite element (FE) method, which has grown hugely over the previous decades, both in the size of domains modelled and the accuracy of the results. A consequence is that these have uncovered new, unexpected behaviour which needs to be understood, of which the waves discussed above form an important example. The early cases of the use of FE in the late 1980s and early 1990s were relatively isolated and were necessarily small given hardware constraints (e.g. [1, 2]), then in the 2000s, as computational power increased, the potential of simulations was exploited for developments in ultrasound in areas such as air-coupled systems, guided wave approaches and visco-elastic systems [3, 4, 5, 6]. Through the development of new techniques, including graphics-card-based simulation tools [7], numerical methods in recent years have delivered important advances in areas requiring high-fidelity wavefield modelling, including Monte Carlo studies of scattering from rough cracks [8], geometrical inversion techniques [9], 3D simulations of guided waves in composites [10], 3D simulations of feature-guided waves [11], high-order guided wave mode thickness measurement [12], super-resolution imaging [13] and high accuracy guided-wave tomographic inversions [14, 15]. Of particular note is that multi-billion degree-of-freedom 3D models for grain scattering have been run, minimising errors to the order of 0.01% in wave speed (see Fig. 7 of [16]). Understanding the different waves which exist in such models is critical to the success of mechanical wave simulation across different applications areas including non-destructive evaluation, seismology and medicine.

Such high-fidelity simulations have highlighted the presence of the wave which is the focus of this paper: the longitudinal wave apparently travelling transversely. To the author's knowledge, the

presence of this wave has not been previously recognised, which leaves an important question about whether it is a genuine physical phenomenon, revealed by the increasing accuracy of modern numerical models, or simply a simulation artefact. This paper will use numerical simulations to demonstrate the phenomenon and highlight its important features, but also provide analytical calculations to confirm it is genuine. This knowledge is vital for numerical models (potentially as well as very accurate experiments) because the presence of an unexpected wave mode could indicate a fundamental error in the excitation or measurement approach which needs to be addressed, possibly at significant cost, so understanding that this occurs and when it does so is important. The consequences of the wave's existence must also be established: what impact does it practically have when it begins interacting with other objects?

This paper will firstly demonstrate the presence of the wave with the FE method in Sect. 2, and an analytical model will explain the origin of the wave in Sect. 3. Section 4 will analyse the scattering behaviour of this wave, then Sect. 5 will evaluate the behaviour of sources for guided waves.

2 Demonstration of the phenomenon via numerical modelling

2.1 Model setup

Numerical modelling is used to demonstrate the behaviour of the waves radiating from a point source. The physical setup, illustrated in Fig. 1, was taken to be a 2D plane strain elastic medium, with a point source at its centre: a force acting in the x direction, which was excited with 3 cycles (Hann windowed) of a 1.5MHz sinusoidal excitation. The material was set to have properties of steel, with Young's modulus 210GPa, shear modulus 80GPa and density 8000kg/m³; at the centre frequency the longitudinal and shear wavelengths become 4mm and 1.6mm respectively. Time trace measurements were taken at two locations: A which is 10mm across in x , and B which is offset 10mm in the y direction.

A finite element elastodynamic simulation was used to simulate the wavefield, with a mesh of element size 0.05mm in both dimensions, and 1200 4-noded linear quad elements in each direction giving a grid of 60×60mm²; this element size gives 81 elements per wavelength for the longitudinal waves and 33 for the shear wavelength. These elements had reduced integration with hourglass control. A time step of 6.6ns was selected, giving a Courant number of 0.8, and absorbing boundaries using the Stiffness Reduction Method [17] were applied to all four boundaries over a 12mm (3λ at the centre

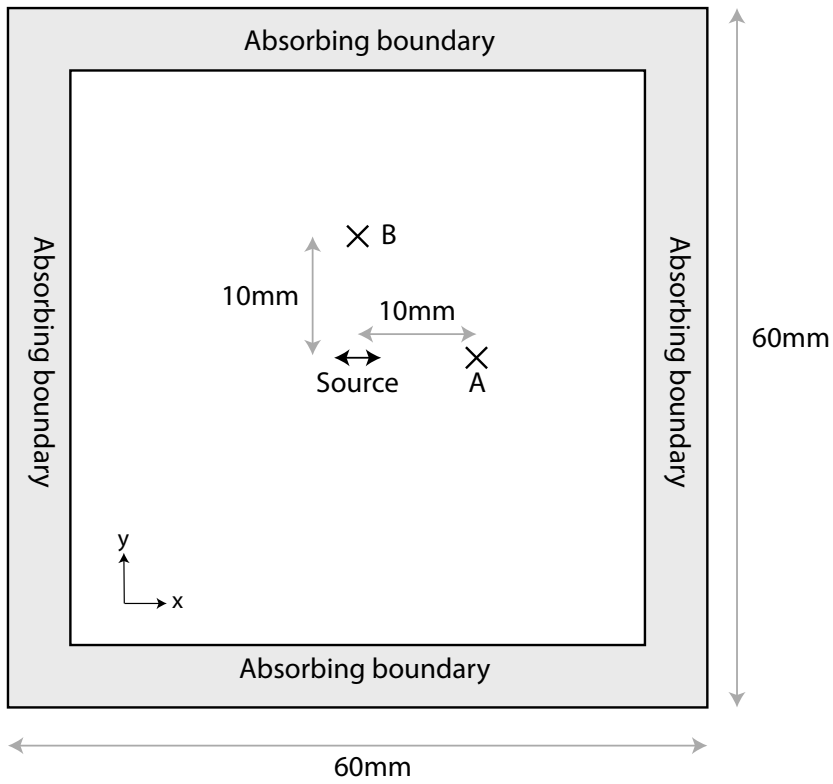


Figure 1: Initial 2D model for demonstrating the presence of the perpendicularly travelling longitudinal wave.

frequency for longitudinal waves) distance. The graphics-card-based explicit time domain solver Pogo was used to solve this [7]; on an Nvidia GeForce GTX 1080 Ti (a consumer card aimed at the gaming market) the 1.44 million-node model with 1362 time increments ran in 3.1 seconds.

2.2 Results

Figure 2 shows the x component of the displacement field at $4\mu\text{s}$; Fig. 2(a) with the colours scaled to capture the full range and Fig. 2(b) with the scale adjusted to significantly clip the peak values and show the presence of both the longitudinal and shear waves at all angles, highlighting the key result of this paper. There are some notable features in these plots. The two wave modes appear to exhibit the same behaviour, with a 90 degree rotation. There is a clear phase advancement of the longitudinal waves along the y axis compared to the waves in the other directions, and this is visible in the shear waves too. The amplitude does drop off significantly in the direction perpendicular to the propagation of longitudinal waves, where one would expect to see no waves of this mode, although as illustrated it does not reach zero, and the same behaviour is true for shear. Figures 2(c) and (d) illustrate the time traces of the x displacement taken at positions A and B from Fig. 2(a) respectively, confirming the results of the field plots; in both perpendicular directions, both modes exist and are clearly measurable. The next section will attempt to mathematically illustrate and explain this.

3 Analytical model

Consider a point excitation in the x direction in a 2D elastic domain. Physically, this will correspond to a force in the x direction, matching the FE simulation in Sect. 2. Taking the scalar potential of the longitudinal wave, this source can be expressed as a dipole of the form

$$s_L(\mathbf{x}) = A_L \frac{\delta(\mathbf{x} - \mathbf{x}_0 - \epsilon\mathbf{i}) - \delta(\mathbf{x} - \mathbf{x}_0 + \epsilon\mathbf{i})}{k\epsilon} \quad (1)$$

assumed centred at \mathbf{x}_0 and with a small spacing of 2ϵ between the two component point sources. k is the wavenumber, \mathbf{i} , \mathbf{j} will be used as standard unit vectors in the x and y directions respectively, and A_L describes the strength of this source. Similarly, the shear potential source will be described as

$$s_S(\mathbf{x}) = A_S \frac{\delta(\mathbf{x} - \mathbf{x}_0 - \epsilon\mathbf{j}) - \delta(\mathbf{x} - \mathbf{x}_0 + \epsilon\mathbf{j})}{k_{sh}\epsilon} \quad (2)$$

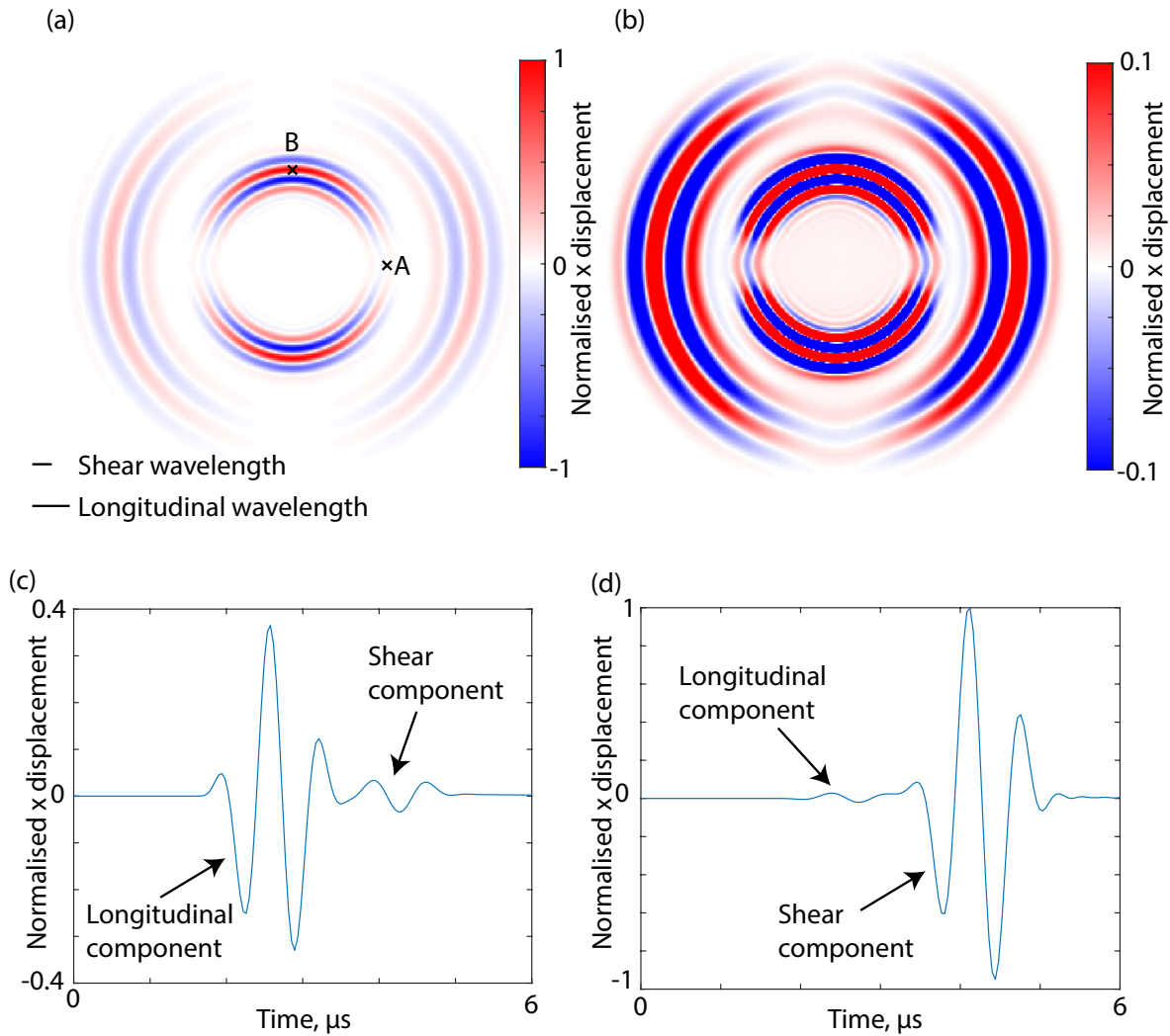


Figure 2: x displacement values of the finite element simulation of a point source, with displacement values scaled relative to the peak displacement at $4\mu s$. (a) shows the field at $4\mu s$ colours scaled across the full range while (b) shows the scale adjusted to 10% such that the presence of the longitudinal and shear components in all directions are visible. (c) and (d) plot the x direction time traces measured at points A and B marked in (a) respectively.

with A_S being the shear wave source strength. For now just the longitudinal component will be considered, which will be independent of the shear. The field radiated from a single unit point source is the Green's function, which in 2D free space becomes

$$G(\mathbf{x} - \mathbf{x}_0) = H_0^{(1)}(k|\mathbf{x} - \mathbf{x}_0|) \quad (3)$$

or taking the radius $r = |\mathbf{x} - \mathbf{x}_0|$ as being larger than a wavelength then this can be approximated as

$$G_\infty(\mathbf{x} - \mathbf{x}_0) = \Pi \frac{e^{ikr}}{\sqrt{r}} \quad (4)$$

with

$$\Pi = \frac{e^{-i\pi/4}}{\sqrt{8\pi k}}.$$

Applying this to the dipole source, the constant Π will be dropped, parameters set as $A_L = 1$, and $\mathbf{x}_0 = \mathbf{0}$ and the two radii expressed as $r_a = |\mathbf{x} - \epsilon\mathbf{i}|$ and $r_b = |\mathbf{x} + \epsilon\mathbf{i}|$ to give the scalar potential of the field as

$$\phi = \frac{e^{ikr_a}}{k\epsilon\sqrt{r_a}} - \frac{e^{ikr_b}}{k\epsilon\sqrt{r_b}}. \quad (5)$$

Since the separation ϵ is small, the slight discrepancy between radii in the denominator terms can be neglected, i.e. let $r \approx r_a \approx r_b$

$$\phi = \frac{e^{ikr_a} - e^{ikr_b}}{k\epsilon\sqrt{r}} \quad (6)$$

then for the exponential parts the approximations $r_a \approx r - \epsilon \cos \theta$ and $r_b \approx r + \epsilon \cos \theta$ can be utilised, with θ being the angle of position \mathbf{x} relative to the x axis. Incorporating this,

$$\phi = e^{ikr} \frac{e^{ik\epsilon \cos \theta} - e^{-ik\epsilon \cos \theta}}{k\epsilon\sqrt{r}} \quad (7)$$

which becomes

$$\phi = e^{ikr} \frac{2i \sin(k\epsilon \cos \theta)}{k\epsilon\sqrt{r}}. \quad (8)$$

Then, since $k\epsilon$ is small, the approximation $\sin \alpha = \alpha$, which is valid at the asymptote, can be used to simplify this to:

$$\phi = e^{ikr} \frac{2i \cos \theta}{\sqrt{r}}. \quad (9)$$

Now consider what would happen on the y axis, where $\theta = \pi/2$. At this point, $\cos\theta = 0$ so the final result is $\phi_L = 0$. This result in the potential field clearly does drop down to zero, which is the intuitive expectation. However, it is now possible to investigate what happens to the displacement field itself at this location. This is defined as

$$\mathbf{u} = \nabla\phi + \nabla \times \boldsymbol{\psi}. \quad (10)$$

The shear component, $\boldsymbol{\psi}$, will continue to be ignored for now and just the $\nabla\phi$ term considered. In polar coordinates this becomes

$$\mathbf{u}_L = \nabla\phi = \frac{\partial\phi}{\partial r}\mathbf{e}_r + \frac{1}{r}\frac{\partial\phi}{\partial\theta}\mathbf{e}_\theta \quad (11)$$

$$= 2i\cos\theta\left(\frac{ik e^{ikr}}{\sqrt{r}} - \frac{e^{ikr}}{2r\sqrt{r}}\right)\mathbf{e}_r + \frac{1}{r}\frac{2i}{\sqrt{r}}e^{ikr}(-\sin\theta)\mathbf{e}_\theta \quad (12)$$

$$= \frac{-2}{\sqrt{r}}e^{ikr}\left[\left(k + \frac{i}{2r}\right)\cos\theta\mathbf{e}_r + \frac{i}{r}\sin\theta\mathbf{e}_\theta\right] \quad (13)$$

Here \mathbf{e}_r and \mathbf{e}_θ are unit vectors in the radial and circumferential directions respectively. It is clear from this that the \mathbf{e}_r component, like the scalar potential, disappears to zero at $\theta = \pi/2$ due to the $\cos\theta$ dependence. However, the \mathbf{e}_θ term does not; along the y axis the values become

$$\mathbf{u}_L(\theta = \pi/2) = -\frac{2ik}{r^{3/2}}. \quad (14)$$

At this point $\mathbf{e}_\theta = \mathbf{i}$, i.e. this component is aligned with the x axis so the wave oscillation will be in this direction. The wave also drops off in amplitude by a factor of $1/r$, in addition to the $1/\sqrt{r}$ which occurs with beam spread, and the additional i factor causes a phase shift of $+\pi/2$ relative to the main wave in the \mathbf{e}_r direction, dominated by the k term. This matches the behaviour identified in Sect. 2. Before establishing the consequences of this, the analysis is completed by discussing the shear wave. Following the logic for the longitudinal waves, the dipole field for the shear source can be described as

$$\psi_z = e^{ik_s r} \frac{2i\sin\theta}{\sqrt{r}} \quad (15)$$

where k_s is the shear wavenumber, and just the out-of-plane, z , component ψ_z is considered to be nonzero for this 2D problem. Utilising the derivation of curl in polar coordinates:

$$\mathbf{u}_S = \nabla \times \boldsymbol{\psi} = \frac{1}{r}\frac{\partial\psi_z}{\partial\theta}\mathbf{e}_r - \frac{\partial\psi_z}{\partial r}\mathbf{e}_\theta \quad (16)$$

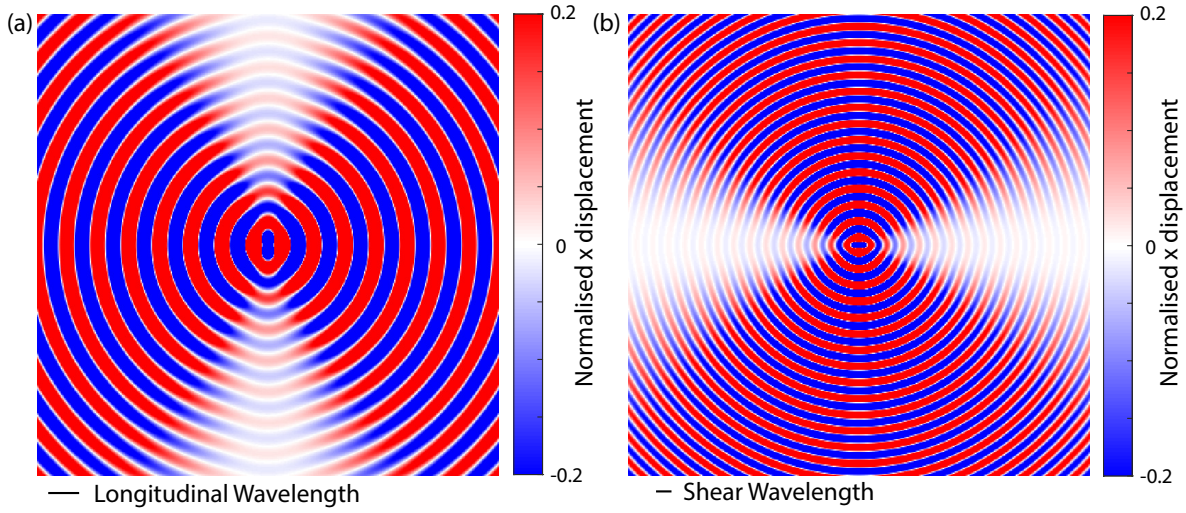


Figure 3: Analytical wavefield solutions for (a) longitudinal and (b) shear waves, given by eqs. (13) and (18) respectively, calculated in steel (properties given in Sect. 2) at 1.5MHz. Colours for both wavefields are clipped to 20% of the peak amplitude measured at 5 wavelengths from the source.

$$= \frac{1}{r} \frac{2i}{\sqrt{r}} e^{ik_s r} \cos \theta \mathbf{e}_r - 2i \sin \theta \left(\frac{ik_s e^{ik_s r}}{\sqrt{r}} - \frac{e^{ik_s r}}{2r\sqrt{r}} \right) \mathbf{e}_\theta \quad (17)$$

$$= \frac{2}{\sqrt{r}} e^{ik_s r} \left[\frac{i}{r} \cos \theta \mathbf{e}_r + \left(k_s + \frac{i}{2r} \right) \sin \theta \mathbf{e}_\theta \right]. \quad (18)$$

Perhaps unsurprisingly, the equation is clearly very similar to eq. (13) derived for the longitudinal waves; the differences are that the system is rotated by $\pi/2$ and the shear wavenumber is used rather than longitudinal.

Figure 3 plots the calculated fields for the longitudinal (Fig. 3(a)) and shear (Fig. 3(b)) components. Both illustrate similar behaviour to that visible in the equivalent FE solution, Fig. 2, although it is noted that the FE solution is a single frame of a time domain simulation while the analytical version is a single frequency solution, i.e. is solved for a continuous wave. As before, there is a clear advance in the wave propagating perpendicular to the main direction of travel (will be referred to as the “perpendicular wave” for the rest of this discussion), reflecting the additional i term causing a phase shift in this component, confirming the FE behaviour.

There are some interesting observations which can be made. On one level this could be considered a near field effect; the relative drop off of $1/kr$ means that its effect will halve as distance from the source is doubled, so at very large distances it will not be significant. However, such identification of “near” and “far” fields are usually reserved for distinct regions of behaviour, which is not the case here, so this is less appropriate.

If there was an infinite line source in the x direction then the derivative of the longitudinal potential field in x must become zero, i.e. $\partial\phi/\partial x = 0$, since there can be no variation in this direction. This means that the corresponding displacement must drop to zero, and therefore the perpendicular wave will not exist. As a result, the perpendicular wave must occur because the wavefield is not straight, i.e. it is the curvature of the wavefield which causes the derivative to be nonzero and hence produces the measurable component. The presence of the $1/r$ factor is therefore unsurprising; it indicates that the strength of the component is inversely proportional to the radius of curvature. Therefore, it is possible to also predict that for any wave of this form, any curvature will result in a visible wave appearing as the derivative becomes nonzero.

It is possible to hypothesise physical justifications for the presence of the component. It could be considered a diffractive effect, where the wavefronts curve around to join up with each other. The two halves of the domain have symmetrical wavefields and diffraction conspires to, in effect, fill the join between them. It should be recognised that for this to be attributed to diffraction, the effect should not be present in the geometrical regime, i.e. at high frequencies. In both eqs. (13) and (18) at large frequencies, k and k_{sh} will be large, and thus dominate the equation, leaving the perpendicular wave component to vanish to zero in the geometric limit. This acts as a mathematical confirmation that the phenomenon can be considered a form of diffraction.

4 Scattering of wave

Previously it has been seen that the longitudinal wave is measurable at a location perpendicular to the source direction; this is the case both in numerical simulations and the equivalent analytical solution. However, this does raise a question about what the consequences are for the behaviour of the wave, i.e. while it can clearly be measured at this location, what, if any, effect will it have when it interacts with an object?

To evaluate this, a set of test simulations are introduced, to evaluate how the wave will behave as it meets a point scatterer located at different angular locations. The simulation is set up as illustrated in Fig. 4. A model of size $100 \times 100 \text{mm}^2$ was defined, with a 1.5MHz source positioned 30mm in each dimension from the lower left corner. A small scatterer was then placed a further 30mm from this source at an angle θ which could be adjusted around the source, to enable all angles to be sampled. To form this scatterer, a hollow circle of size 0.2mm was used, which is small enough to be treated as a

point¹. An 8mm absorbing boundary using the SRM [17] was applied around the edges of the domain.

The strength of the resulting scattered field should then be measured. It is noted that the scattered field will vary as a function of the scattering angle relative to the incident wave, so it is important to keep this constant, as well as maintaining the same distance from the scatterer. However, since it is not of interest to obtain absolute values of scattering amplitude, but rather how this changes as the scatterer moves around the source, the specific angle at which the scattered field is measured relative to the source is unimportant, provided it is constant. For these purposes, a scattering angle of 45° was used throughout, as shown in Fig. 4, with the scatterer and its measurement point being rigidly rotated around the source. The 45° angle was selected as this should produce both longitudinal and shear waves and hence avoid any scenario where the receiver was positioned to miss one particular type of wave. The receiver was set to measure displacement in the direction directly aligned with the scatterer as shown in the figure.

Two sets of simulations are run. The first set was as discussed above, and the second was an incident case where the circle was filled but the remainder of the mesh was unchanged, effectively removing the scatterer. The difference between these two cases is taken to give the scattered field, which is the final quantity considered.

A free mesh was used to model the domain, allowing arbitrary positioning of the source, scatterer and receivers. The target element size was set to 0.04mm, to give 100 elements per longitudinal wavelength. The elements were linear triangular plane strain elastic elements. Both the total and incident models were run 101 times each to sweep through all angles of θ from 0° to 100° at 1° intervals. Once loaded, the incident component was subtracted and the signals were windowed to obtain just the first arrivals, corresponding to the longitudinal excited waves scattered to longitudinal at the scatterer. These were Fourier transformed and the component corresponding to 1.5MHz extracted, normalised by dividing by their mean across the 101 values, and plotted.

Figure 5 shows a comparison between the scattered field measured and the different wave components calculated analytically in Sect. 3. These demonstrate how the scattered field is clearly following the pattern of the wavefield potential, rather than the x component of the wave, notably passing through zero amplitude at the 90° point. This indicates that the wave propagating in the perpendicular direction does not scatter, despite existing as a displacement. This leads to an interesting, somewhat philosophical, conclusion: while the wave does exist at that location, in that it is clearly

¹The author has also demonstrated identical behaviour with a scatterer formed by fixing both x and y displacements but these results are not presented here.

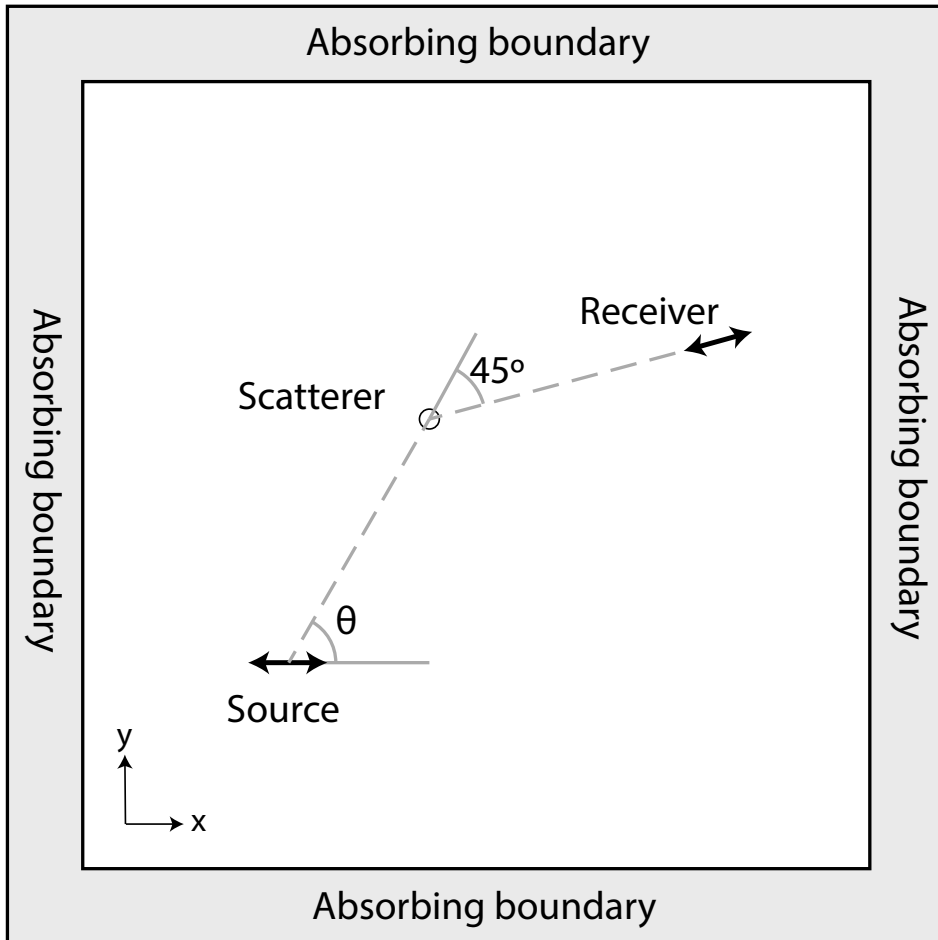


Figure 4: Schematic of model to test scattering behaviour in all directions. The scatterer and receiver are rotated rigidly around the source.

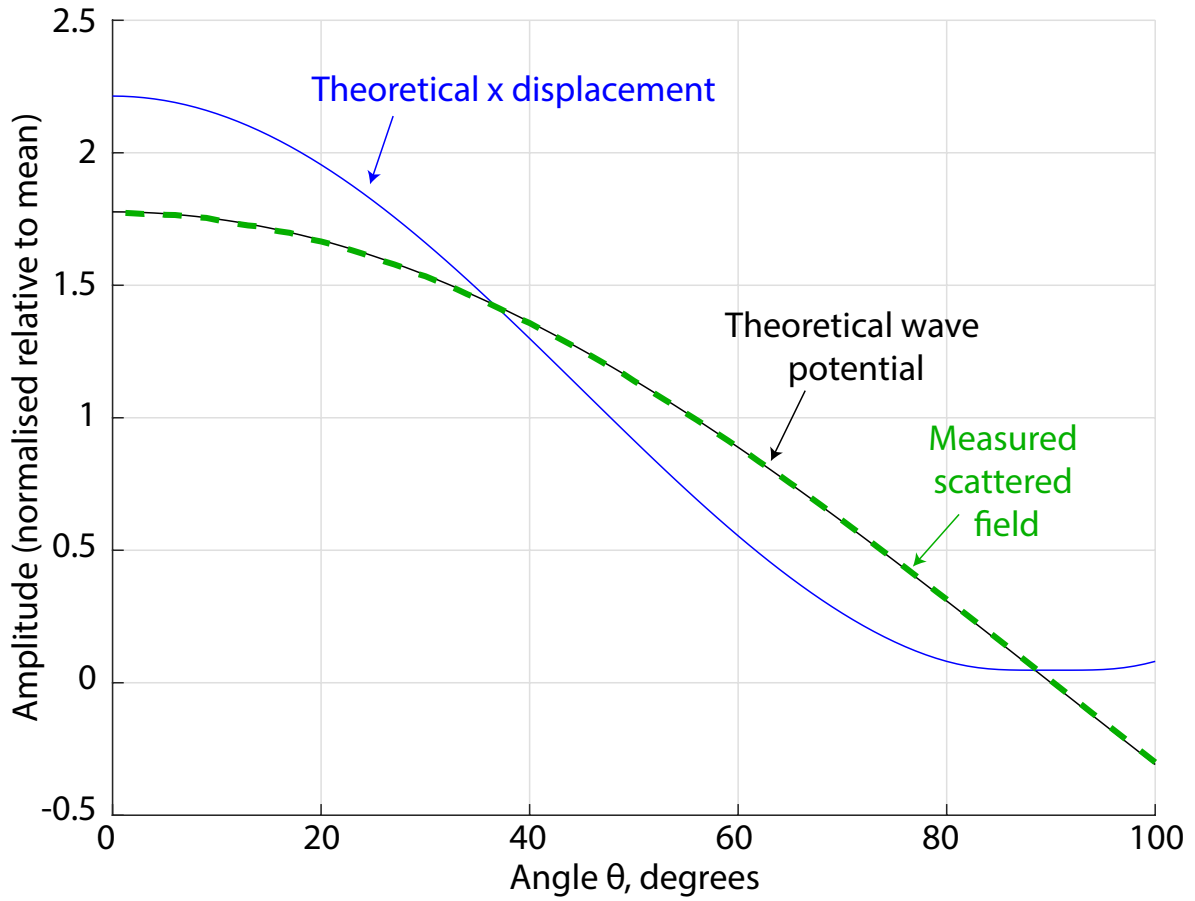


Figure 5: The measured scattered field from the setup of Fig. 4 compared to the theoretically calculated values for wave potential from eq. (9) and displacement from resolving eq. (13) into the x direction.

measurable, it does not exist in that it does not cause any scattering.

Hypothesising about the reason for this behaviour, it can be stated that the underlying scalar potential is the fundamental quantity, and the physical displacement fields produced arise as a result of this potential field. Based on this, it would seem logical that scattering would be proportional to this scalar potential rather than any other derived quantity, even though the scalar potential is not directly measurable itself.

5 Guided wave demonstration

Guided waves have important applications within NDE, having some desirable properties including their ability to propagate large distances with minimal amplitude loss, enabling large components to be inspected. The phenomenon described in this paper also exists for guided waves in plates for the S0 and SH0 waves; physically this is unsurprising since an S0/SH0 model can be captured well in the low frequency regime by 2D plane stress behaviour, and the only practical difference between this and plane strain considered for bulk waves is that the effective stiffnesses change. This section will provide a confirmation of this behaviour through numerical modelling, as well as including analysis of the A0 mode.

A finite element model was again set up, a 3D plate of 10mm thickness (z direction) and extent 2m in the in-plane directions, x and y , as illustrated in Fig. 6(a). A 1N force was excited in the x direction, centred in the the x and y directions and applied to the top surface of the plate; this was a Hann-windowed toneburst of 3 cycles and a centre frequency of 50kHz. This excitation will excite all three of the fundamental modes, A0, S0 and SH0. The element size was set to 2mm in each dimension giving over 60 8-node linear brick elements per longitudinal bulk wavelength and 31 for shear, which should be more than sufficient for the resulting guided waves, and the time step was $0.165\mu\text{s}$ targeting a Courant number of 0.5. No absorbing boundaries were used in this model.

Figures 6(b), (c) and (d) show the scalar potentials for the three different modes present, A0, SH0 and S0, calculated from the output displacement fields in x , y and z . The A0 mode was extracted by taking the difference in the divergence in x and y on the top and bottom surfaces, S0 was extracted from the difference between the z components on top and bottom surfaces, and SH0 was taken as the curl in x and y at the central plane of the plate. In all cases the necessary differentials were calculated as simple first-order finite differences between adjacent nodes on the grid. In each case the behaviour is as expected; the potential disappears to zero (and the sign changes) perpendicular to the direction

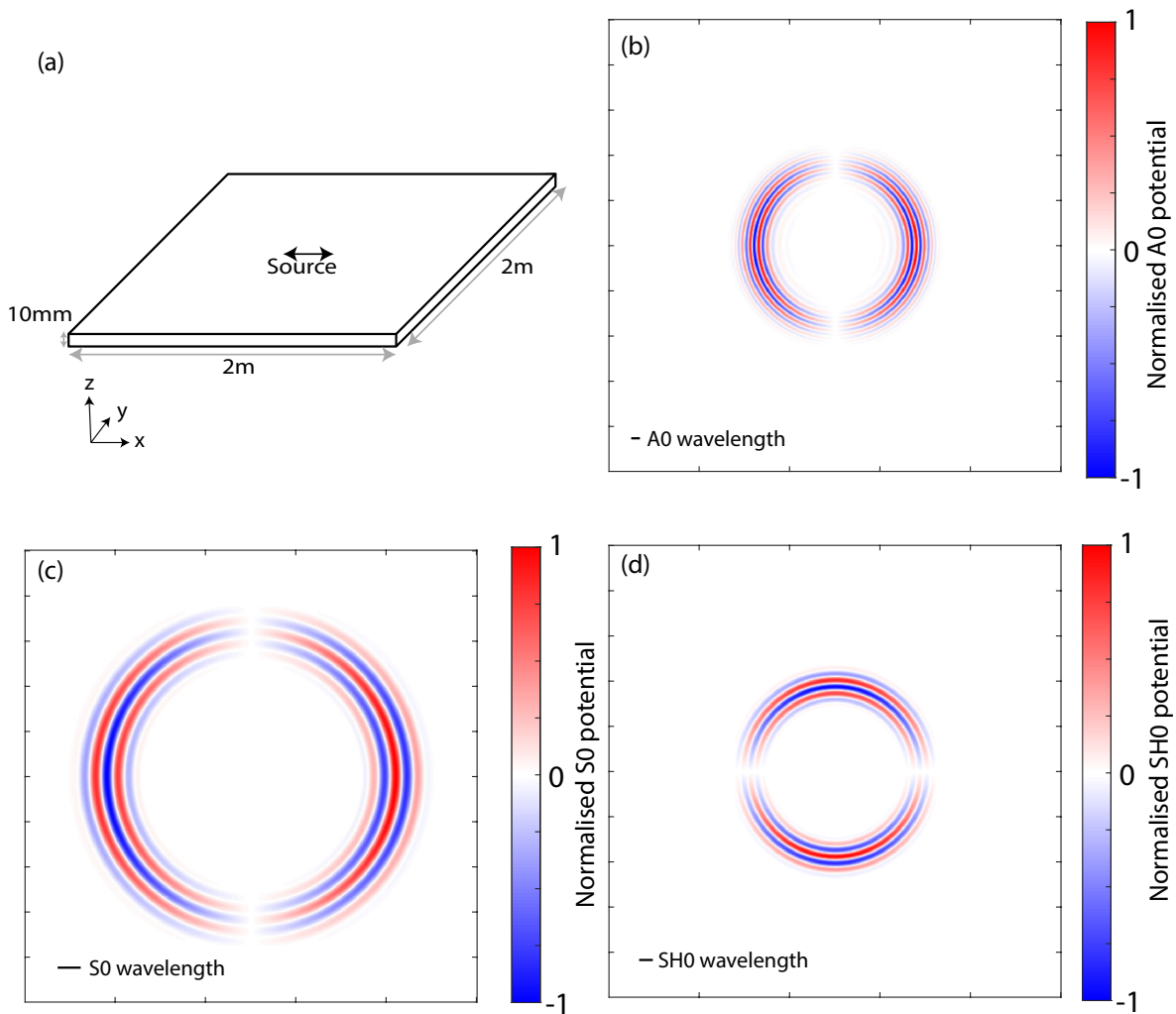


Figure 6: (a) Illustration of the physical guided wave model. Guided wave scalar potentials for (b) A0, (c) S0, (d) SH0, normalised relative to their respective peaks. These are taken at a time of $151\mu\text{s}$.

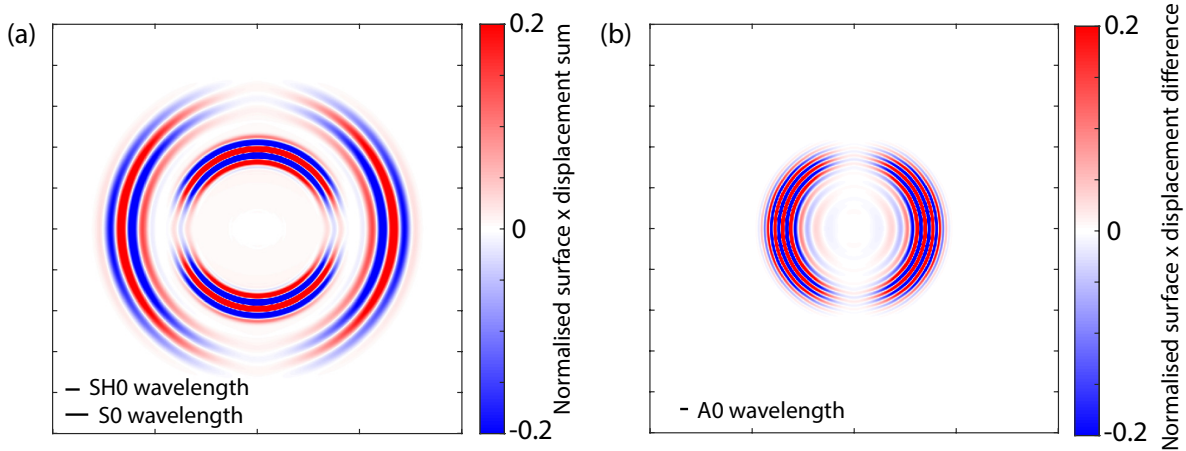


Figure 7: x displacement values (a) summed on the top and bottom surface to show SH0 and S0, (b) bottom surface subtracted from top to show A0. Both plots are normalised against their respective peaks, and the colours are then clipped to 20% of the maximum.

of propagation.

Figure 7 then illustrates the displacements which correspond to the scalar potentials. While plotting the top x displacement would be sufficient to visualise the waves, the A0 and SH0 waves have similar velocities at this frequency-thickness and would overlap. To address this, the asymmetry of A0 versus the symmetry of SH0 have been exploited to separate: the sum of displacement on top and bottom is illustrated in Fig. 7(a) capturing the symmetry of S0 and SH0, and the displacement difference is shown in Fig 7(b) capturing just A0.

In all three cases the colour scale has been adjusted so that the presence of the perpendicularly travelling component is clearly visible. As discussed previously, this is to be expected for the S0 and SH0 modes via the plane strain/plane stress argument. However, it appears for the bending mode A0 too.

As a generalisation of the principle, there are two key aspects which can be identified from the derivation of Sect. 3 as being necessary for the presence of the “perpendicular wave” to exist:

1. The source must form a dipole within the scalar formulation for that specific wave.
2. The physical wavefield must be some form of derivative of the underlying scalar potential.

The first rule provides the zero in the direction perpendicular to the primary direction of travel, but the derivative itself will not be zero, such that the second rule enables a wave to be physically measured. The dipolar source implies that the wave must be polarised. This can be either a transverse wave or

longitudinal, i.e. direction of motion is the same as the direction of propagation; through this paper both forms have been demonstrated, as well as the A0 mode which is a combination of both forms.

6 Conclusions

This paper has identified and explained a counter-intuitive wave component which propagates perpendicularly to the expected direction of propagation, and highlighted its existence for both longitudinal and shear waves, as well as for guided waves in plates. The underlying wavefield potentials, arising from the Helmholtz decomposition, do reduce to zero in the perpendicular direction as expected, but since their derivatives do not, the physical displacement itself does not. The waves have interesting properties: while they are demonstrably measurable, they do not scatter, and it has been shown that they are caused through a diffractive effect. Thoroughly uncovering the phenomenon is critical for the reliable use of high-fidelity numerical simulations.

This wave phenomenon is also likely to occur with other physical modalities which are polarised, provided the source forms a dipole in the scalar potential and that the physical wavefield is then a derivative of this. This should be the case with electromagnetic waves, although such investigations are beyond the scope of this paper.

7 Acknowledgements

The author would like to thank Mike Lowe, Peter Cawley, Stefano Mariani and Euan Rodgers variously for raising the issue initially, discussions around the phenomenon and comments on the draft of this paper.

8 Data availability

The scripts to generate the finite element models and recreate the results from this work are available from [Supplementary material].

References

- [1] R. Ludwig and W. Lord, “A Finite-Element Formulation for the Study of Ultrasonic NDT Systems,” *IEEE Transactions on Ultrasonics, Ferroelectrics, and Frequency Control*, vol. 35, no. 6, pp. 809–820, 1988.
- [2] D. N. Alleyne and P. Cawley, “The Interaction of Lamb Waves with Defects,” *IEEE Transactions on Ultrasonics, Ferroelectrics, and Frequency Control*, vol. 39, no. 3, pp. 381–397, 1992.
- [3] M. Castaings, C. Bacon, B. Hosten, and M. V. Predoi, “Finite element predictions for the dynamic response of thermo-viscoelastic material structures,” *The Journal of the Acoustical Society of America*, vol. 115, pp. 1125–1133, mar 2004.
- [4] P. Rajagopal and M. J. S. Lowe, “Scattering of the fundamental shear horizontal guided wave by a part-thickness crack in an isotropic plate,” *The Journal of the Acoustical Society of America*, vol. 124, pp. 2895–2904, nov 2008.
- [5] W. Ke, M. Castaings, and C. Bacon, “3D finite element simulations of an air-coupled ultrasonic NDT system,” *NDT and E International*, vol. 42, pp. 524–533, sep 2009.
- [6] J. Zhang, B. W. Drinkwater, and P. D. Wilcox, “Longitudinal wave scattering from rough crack-like defects,” *IEEE Transactions on Ultrasonics, Ferroelectrics, and Frequency Control*, vol. 58, pp. 2171–2180, oct 2011.
- [7] P. Huthwaite, “Accelerated finite element elastodynamic simulations using the GPU,” *Journal of Computational Physics*, vol. 257, pp. 687–707, jan 2014.
- [8] S. G. Haslinger, M. J. Lowe, P. Huthwaite, R. V. Craster, and F. Shi, “Elastic shear wave scattering by randomly rough surfaces,” *Journal of the Mechanics and Physics of Solids*, vol. 137, p. 103852, apr 2020.
- [9] F. Shi and P. Huthwaite, “Waveform-Based Geometrical Inversion of Obstacles,” *Physical Review Applied*, vol. 12, p. 064008, dec 2019.
- [10] C. A. Leckey, M. D. Rogge, and F. Raymond Parker, “Guided waves in anisotropic and quasi-isotropic aerospace composites: Three-dimensional simulation and experiment,” *Ultrasonics*, vol. 54, pp. 385–394, jan 2014.

- [11] X. Yu, P. Zuo, J. Xiao, and Z. Fan, “Detection of damage in welded joints using high order feature guided ultrasonic waves,” *Mechanical Systems and Signal Processing*, vol. 126, pp. 176–192, jul 2019.
- [12] P. Belanger, “High order shear horizontal modes for minimum remnant thickness.,” *Ultrasonics*, vol. 54, pp. 1078–87, apr 2014.
- [13] J. B. Elliott, M. J. Lowe, P. Huthwaite, R. Phillips, and D. J. Duxbury, “Sizing Subwavelength Defects with Ultrasonic Imagery: An Assessment of Super-Resolution Imaging on Simulated Rough Defects,” *IEEE Transactions on Ultrasonics, Ferroelectrics, and Frequency Control*, vol. 66, pp. 1634–1648, oct 2019.
- [14] P. Huthwaite, “Guided wave tomography with an improved scattering model,” *Proceedings of the Royal Society A: Mathematical, Physical and Engineering Science*, vol. 472, no. 2195, p. 20160643, 2016.
- [15] A. A. E. Zimmermann, P. Huthwaite, and B. Pavlakovic, “High-resolution thickness maps of corrosion using SH1 guided wave tomography,” *Proceedings of the Royal Society A: Mathematical, Physical and Engineering Sciences*, vol. 477, p. 20200380, jan 2021.
- [16] M. Huang, G. Sha, P. Huthwaite, S. I. Rokhlin, and M. J. S. Lowe, “Maximizing the accuracy of finite element simulation of elastic wave propagation in polycrystals,” *The Journal of the Acoustical Society of America*, vol. 148, pp. 1890–1910, oct 2020.
- [17] J. R. Pettit, A. Walker, P. Cawley, and M. J. S. Lowe, “A Stiffness Reduction Method for efficient absorption of waves at boundaries for use in commercial Finite Element codes.,” *Ultrasonics*, vol. 54, pp. 1868–79, sep 2014.